Nanoscale characterisation of TiO2(110) annealed in air

Sasahara, Akira
Murakami, Tatsuya
Tu, Le Tran Uyen
Tomitori, Masahiko

(Citation)
Applied Surface Science,428:1000-1005

(Issue Date)
2018-01-15

(Resource Type)
journal article

(Version)
Accepted Manuscript

(URL)
https://hdl.handle.net/20.500.14094/90004618

Nanoscale Characterisation of TiO_2(110) Annealed in Air

Akira Sasahara, Tatsuya Murakami, Le Tran Uyen Tu, and Masahiko Tomitori*

Japan Advanced Institute of Science and Technology, Nomi, Ishikawa 923-1292, Japan

*To whom correspondence should be addressed.

E-mail: sasahara@harbor.kobe-u.ac.jp

Present address: Department of Chemistry, Faculty of Science

Kobe University

Nada-ku, Kobe 657-8501, Japan

Tel: +81-78-803-5674

Fax: +81-78=803-5674

Abstract

Rutile titanium dioxide (TiO_2) (110) surfaces annealed in air were examined by frequency modulation atomic force microscopy (FM-AFM), X-ray photoelectron spectroscopy (XPS) and low-energy electron diffraction (LEED) techniques. The terraces separated by monatomic steps showed an atomically irregular appearance in the obtained FM-AFM images, while the surface produced a (1 × 1) LEED pattern that indicated atomic ordering of the top few surface layers. Subsequent annealing in atmospheric-pressure O_2 produced several ten-nanometre-sized pits with irregular shapes on the terraces. Molecule-sized spots were recognised on the subsequently O_2-annealed surface. Half-order spots along the <001> directions emerged in the LEED pattern. We propose the rutile substrate covered with hydroxylated amorphous TiO_2 of monatomic thickness as the structure of the air-annealed surface. The amorphous TiO_2 was dehydroxylated by subsequent O_2 annealing and was transformed into the thermodynamically stable rutile structure. The molecule-sized spots were attributed to hydroxyl (OH) and hydroperoxyl (OOH) groups that were produced on the area with the (1 × 1) structure. A part of the OH and OOH groups were arranged in a (2 × 1) structure and produced the half-order spots in the LEED pattern.

Keywords

TiO_2, rutile, amorphous, atomic force microscopy

Introduction

Rutile titanium dioxide (TiO_2) single-crystal wafers have been used in surface science studies of TiO_2 because of their high crystallographic quality, ease of experimental handling, and commercial availability [1,2]. Nanocrystalline TiO_2 for industrial applications is subjected to several heat treatments in oxidative environments, such as fusing, calcining and sintering. Hence, a TiO_2 single-crystal surface annealed in air represents a potentially realistic model of TiO_2-based products using nanocrystalline TiO_2, such as catalysts, electrodes and medical implants. Among the rutile TiO_2 single-crystal surfaces, the (110) surface has been most widely studied. This is reasonable considering that the thermodynamically stable {110} facet is dominant in rutile TiO_2 nanocrystals [2].

Kielbassa et al. showed that the sintering of Au particles supported on an air-annealed (110) surface was promoted when an oxidative atmosphere was used rather than a vacuum [3]. Eyrich et al. reported that the turnover frequency for catalytic CO oxidation on Au/TiO_2(110) surfaces was increased by a factor of ten when the air-annealed surface was reduced in ultrahigh vacuum (UHV) before Au evaporation [4]. The segregation of Ti interstitials from the bulk to the surface was proposed to enhance the photocatalytic activity of such a system. Dohshi et al. reported that the air-annealed (110) surface showed a hydrophobicity lower than that of the air-annealed (100) surface upon irradiation of the two surfaces by γ-rays and by UV light [5]. The structure-sensitive photocatalytic activity that led to the decomposition of organic contaminants was concluded as a major reason for the difference in hydrophilicity. The surface-orientation-dependent photocatalytic activity was also reported by Yamamoto et al. [6]. The air-annealed (101) surface exhibited the highest activity in the reduction of aqueous Ag^+ relative to those of other low-index surfaces, including the (110), (100), (001) and (111) surfaces.

Nanoscale views of the air-annealed (110) surface may help provide a thorough understanding of the chemical processes occurring therein and therefore may aid in improving product performance. The air-annealed surface is known to exhibit a step-terrace structure with a stoichiometric composition [4,7]. However, nanostructures of the surface have not yet been examined. Unidentified contaminants from laboratory air have made the nanoscale characterisation of the surface unfeasible. The non-conductivity of the air-annealed surface also restricts analytical methods. Many surface sensitive analytical techniques employ charged particles, such as electrons and ions, as probes; because of the inherent charging, they are therefore unsuitable for analysing the air-annealed surface.

Although the nanostructures of the air-annealed rutile TiO_2(110) surface are unclear, the (110) surface subjected to sputtering–annealing cycles in a UHV has been revealed to exhibit an atomically well-ordered (1 × 1) structure corresponding to a truncation of the bulk crystal. Here, we viewed the (1 × 1) surface in order to examine the nanostructures of the air-annealed surface. We use the phrase '(1 × 1)' surface in this article only to indicate the sputter-annealed (110) surface, although the air-annealed (110) surface also produces a (1 × 1) low-energy electron diffraction (LEED) pattern, as presented later.

Figure 1a shows the model of the (1 × 1) surface [8–10]. The (1 × 1) surface is characterised by the protruding [001]-directed rows of O atoms bridging two Ti atoms (O_b atoms) and the Ti atoms coordinated to five O atoms (Ti_{5c} atoms) exposed at the troughs between the O_b atom rows. Some of the O_b atoms are capped by H atoms, which thus form OH groups (OH_b groups) that are produced by the dissociation of residual H_2O molecules in the UHV chamber [8]. Some of the remaining O_b atoms are missing, that is, O vacancies have been formed. The dimensions of the unit cell that involves two Ti atoms and four O atoms are 0.30 nm × 0.65 nm. The OH_t group in Figure 1a is another type of OH group that terminates the Ti_{5c} atoms. The OH_t groups are produced by the reaction of the OH_b groups with O adatoms [11]. Therefore, the OH_t groups are not present on the (1 × 1) surface in the O_2-free UHV environment. The OH_t groups were, however, found on the (1 × 1) surface when the surface was re-introduced into the UHV after exposure to laboratory air [12]. The sputtering–annealing cycles produce defects such as O vacancies and Ti interstitials in the bulk crystal, thereby converting the TiO_2 wafer with the (1 × 1) surface into an n-type semiconductor [13].

The nanoscale features of the (1 × 1) surface can be visualised by scanning probe microscopy techniques such as scanning tunnelling microscopy (STM) [8–10] and frequency modulation atomic force microscopy (FM-AFM) [14,15]. Figure 1b shows an FM-AFM image of the wide-field view of the (1 × 1) surface in UHV. FM-AFM used an atomic force acting on the probe tip in order to regulate the probe–sample distance [16]. Unlike STM, FM-AFM does not require electrical conductivity of the sample. Therefore, FM-AFM is applicable to analysis of the insulating air-annealed TiO_2 surfaces. The area in Figure 1b includes three wide terraces separated by two major steps, extending roughly oriented in the [001] direction. Islands and pits can be observed on the wide terraces. The heights of the major steps and islands and the depth of the pits are 0.35 ± 0.03 nm, which is comparable to that of the monatomic step of the (110) surface, 0.32 nm. In a close-up of the terrace, shown in Figure 1c, the protruding O_b atom rows are observed as bright rows along the

[001] direction. The bright protrusions and the depression in the O_b atom rows are the OH_b groups and the O vacancy, respectively.

Material and methods

Mirror-polished TiO_2(110) wafers (Shinkosha) were ultrasonically degreased in acetone, etched in a 10% aqueous HF solution, and ultrasonically washed with Milli-Q water. The wafers were then annealed at 1273 K for 12 h in a sapphire tube placed in a tube furnace. After the wafers were cooled to room temperature in the sapphire tube, they were introduced into the UHV chambers equipped with FM-AFM, X-ray photoelectron spectroscopy (XPS) and LEED equipment. Subsequent annealing in O_2 was performed in a quartz tube at 773 K for 1 h. The pressure and the flow rate of O_2 were controlled by a gas regulator at 1.3×10^5 Pa and 0.5 L/min, respectively. With these O_2 annealing conditions, Si evaporated from the quartz tube [17,18] was under the detection limit of XPS.

The analysis of these surfaces was then performed at room temperature. FM-AFM images were obtained using a commercial UHV microscope (JSPM4500A, JEOL) with a base pressure of 3×10^{-8} Pa. Silicon cantilevers with a nominal resonance frequency of 315 kHz and a spring constant of 14 N/m (NSC12, MikroMasch) were used as a probe. In order to minimise the long-range electrostatic interaction unfavourable to high-resolution imaging, the average contact potential difference between the TiO_2 wafers and the cantilevers was nullified by applying bias voltages between them. Cross sections smoothed by a nine-point median filter were measured for the images by using WSxM software [19]. LEED patterns were obtained using a commercial optics device (BDL600, OCI) installed in another UHV system with a base pressure of 2×10^{-8} Pa.

XPS spectra were recorded using a commercial instrument (Axis Ultra DLD, Kratos) with a base pressure of 6×10^{-7} Pa. A monochromatic Al Kα line was used as an excitation source, and the charging of the surface was minimised by using a low-energy electron neutraliser. The photoelectron emission angle with respect to the surface normal was set to 0°. The pass energy and energy step were 160 eV and 1.0 eV for wide scans, and 20 eV and 0.1 eV for narrow scans, respectively. The spectra were deconvoluted into mixed Gaussian–Lorentzian curves (expressing 70% Gaussian character) after Shirley-type background subtraction. The binding energy of the spectra was calibrated such that the Ti 2p3/2 peak of TiO_2 was 459.1 eV [20]. With this calibration, the major O 1s peak for the O atoms in the bulk TiO_2 crystal (O_{bulk} atoms) was corrected to 530.3 eV.

Results and discussion

Figure 2a,b shows FM-AFM images of the air-annealed (110) surface. The surface consisted of flat terraces separated by steps extending roughly parallel to each other. The height of the steps was 0.35 ± 0.03 nm, corresponding to the monatomic step shown in the cross section (i) of Figure 2c and similar to the height determined for the (1 × 1) surface. The direction of the steps and the step-to-step distance differed depending on the wafers, which probably reflects a miscut of the surface. These features are consistent with those presented in previous studies [3,4,6]. The terraces showed an irregular morphology with height fluctuations of up to 0.4 nm, as shown in the cross section (ii) in Figure 2c. Although an atomic-scale periodic contrast is not apparent in the FM-AFM images, the surface produced a (1 × 1) LEED pattern, as shown in Figure 2d. Faint half-order spots along the [1$\bar{1}$0] direction, indicated by the arrows, were observed for several wafers. Figure 2e shows a wide-scan XPS spectrum of the surface. The intense peaks at ~460 and ~530 eV are the Ti 2p and O 1s peaks, respectively. Moreover, a C peak from the adventitious organic contaminants was detected. Either or both of Na and K were detected on some of the wafers. The densities of the Na atoms and K atom at their maximum values were ~3.0 and ~2.0 nm^{-2}, respectively, under the extreme assumption that they are both present on the surface. The features observed in the FM-AFM images and LEED patterns were independent of the presence of the Na and K impurities.

One possible interpretation of the irregular topography of the air-annealed surface is that the topmost layer consists of amorphous TiO_2. The (1 × 1) LEED pattern indicates that either the top or the second topmost surface layer possessed a rutile structure, because the escape depth of the low-energy electrons is ~0.6 nm. The second topmost layer must therefore be arranged in a rutile structure. When the second and lower layers crystallise into a rutile structure, the monatomic steps appear, although the topmost layer is amorphous. Figure 3a shows a model of the air-annealed surface. On the basis of diffraction experiments, Petkov et al. concluded that the atom arrangement in amorphous TiO_2 resembles that of brookite TiO_2 [21]. Referring to their work, we determined parts of the TiO_6 octahedra units comprising brookite to be tentatively attached to the rutile substrate. The amorphous fragments (i) and (ii) are depicted in the upper panel of Figure 3b. The edge-sharing TiO_6 octahedra, indicated by asterisks, are attached to the Ti_{5c} atom rows of the (1 × 1) surface. The non-periodic arrangement of the amorphous fragments would thus result in this irregular surface topography. The half-order LEED spots may be explained by the accidental periodic ordering of the fragments in the [1$\bar{1}$0] direction.

According to the model shown in Figure 3a, the rutile substrate with the (1 × 1) structure may be exposed through the breaks in the amorphous fragments. However, such an area in the (1 × 1)

structure is expected to be limited. The (1 × 1) surface has been found to be covered by OH_t groups and hydroperoxyl (OOH) groups when it was re-introduced into UHV from the laboratory air [12]. These surface species are formed by dissociation of H_2O molecules on the (1 × 1) surface and adopt an arrangement with (2 × 1) periodicity. The half-order LEED spots along the [001] direction corresponding to the (2 × 1) periodicity were not found on the air-annealed surface.

The entire topmost layer does not likely consist of organic contaminants distributed on the rutile substrate. The topography of the air-annealed surface markedly changed upon further annealing of the air-annealed surface in O_2, as shown later. The O_2-annealed surface was also exposed to laboratory air during transfer from the quartz tube to the UHV chamber, similarly to the air-annealed surface. The area higher than the surrounding protrusions with an irregular shape are most likely the aggregates of the organic contaminants. Three of such area are indicated by arrowheads in Figure 2b. The overall volume of the areas higher by ≥0.3 nm than the lowest point in Figure 2b was ~70 nm^3. Assuming that the C atoms are spheres with a radius of 0.07 nm, we included 50,000 C atoms in these area. The density of the C atoms in Figure 2b is estimated to be ~20 nm^{-2}. This value roughly corresponds to the density of ~60 nm^{-2} that was calculated from the C 1s and Ti 2p peak intensities by assuming a uniform C layer on the TiO_2 substrate [17].

Next, we considered how amorphous TiO_2, which is thermodynamically unfavourable compared with rutile TiO_2, is stabilised on the topmost layer. According to Shimizu et al., the HF-etched (110) surface exhibited a (1 × 1) structure when annealed in UHV without Ar^+ sputtering [22]. Therefore, some air component gases are responsible for the stabilisation of amorphous TiO_2. The most probable component is H_2O. Yanagisawa et al. proposed that hydroxylation hinders the transformation of amorphous TiO_2 to anatase [23]. The mirror-polished TiO_2 wafers could be covered with thick amorphous layers. The amorphous layers acquire the rutile structure via annealing in air. However, the topmost layer could be stabilised in an amorphous form by hydroxylation during cooling in a humid atmosphere. The polar OH groups locally enhanced the long-range electrostatic interaction between the tip and the sample [24] and might have thus hindered the high-resolution imaging of the surface.

The hypothesis of the OH group-induced topography of the air-annealed surface was examined by subsequent annealing in O_2. Figure 4a,b show the FM-AFM images of the surface (Figure 2) that was further annealed in atmospheric pressure O_2. Several ten-nanometre sized pits with irregular shapes appeared on the terraces. The cross section (i) in Figure 4c shows that the bottom of the pits, marked with arrowheads, reach the level of the lower terrace. Careful examination of Figure 4b

confirmed molecule-sized spots on the terraces. The arrows in the inset indicate the molecule-sized spots. The distance between the arrows along the [1$\bar{1}$0] direction was 0.66 nm and was comparable to the distance between the adjacent Ti_{5c} atom rows. The bright particles indicated by the arrowheads are probably the aggregates of the organic contaminants that were also observed on the air-annealed surfaces. The (1 × 1) LEED spots became sharper with this annealing, as shown in Figure 4d. A closer look at the LEED pattern shows faint spots indicating a (2 × 1) periodicity, as indicated by the arrows. The wide-scan XPS spectrum in Figure 4e looks almost identical to that of the air-annealed surface shown in Figure 2e. Emergence of faint K 2p peaks was confirmed by narrow-scan spectra (the spectra were not shown here). The densities of K, as estimated under the assumption described above, were 1.3 nm^{-2} or less when the O_2-annealed surfaces were prepared from the K-free air-annealed surfaces. K atoms may have a high affinity for O atoms and may therefore be segregated on the surface by annealing in high-pressure O_2.

The assumed structural change of the amorphous fragments induced by annealing in O_2 is illustrated in Figure 3b. The uppermost TiO_6 of the fragment (i) moved to form a linear TiO_6 chain. The linear chain of the edge-sharing TiO_6 formed the (1 × 1) structure. The fragment (ii) also transformed into a linear chain of the edge-sharing TiO_6. Such a transformation of the two corner-sharing TiO_6 octahedra to edge-sharing TiO_6 octahedra involves dehydration and is catalysed by H_2O molecules [25,26]. In the dry O_2 atmosphere, the transformation proceeds by simple dehydration of two hydroxylated TiO_6 octahedra. The rearrangement of TiO_6 could lead to an increase in the area of the (1 × 1) structure. The (1 × 1) area was found to be covered by the OH and OOH groups when the surface was introduced into the UHV. The molecule-sized spots in Figure 4b are assigned to the OH or OOH groups. The OH groups and OOH groups were ordered in a (2 × 1) structure, as indicated by the LEED pattern.

The transformation of amorphous TiO_2 to rutile TiO_2 is accompanied by an 11% increase in density [27,28]. The area of the topmost layer thus decreases by 10% under the assumption that the amorphous topmost layer transforms to the rutile phase without changing its thickness. The re-arrangement of the TiO_6 octahedra composing the topmost layer would not cause a distinct change in the thickness of the layer. The area of the pits in the FM-AFM images was approximately 12% of the surface and is comparable to the decrease in the area caused by a transformation to the rutile phase. Thus, the amorphous-to-rutile transformation can account for the area of the pits.

Conclusions

This work addressed the nanostructures of a rutile TiO_2(110) surface annealed in air. The irregular topography of the surface may be explained by assuming that the rutile substrate is covered with amorphous TiO_2. The topmost layer was transformed into the rutile structure by annealing in O_2. The amorphous TiO_2 on the air-annealed surface is probably stabilised by hydroxylation. Annealing in O_2 dehydroxylates the amorphous TiO_2 and thereby promotes the transformation into rutile TiO_2.

The obtained results may contribute to studies that use the air-annealed surface as a realistic model of commercial nanocrystalline TiO_2. The roles of the surface nanostructures in the industrially useful properties of TiO_2 could be clarified by such model studies, which may lead to the improvement of the TiO_2-based products. Controlling the humidity under ambient conditions during annealing is a possible key to controlling the nanostructures of these wafers.

Acknowledgements

This work was supported by the Grants-in-Aid for Scientific Research from the Japanese Society for the Promotion of Science KAKENHI (grants 26600024, 26630330, 24246014 and 16K13624). We would like to thank Uni-edit (www.uni-edit.net) for editing and proofreading this manuscript.

References

[1] C.L. Pang, R. Lindsay, G. Thornton, Chemical reactions on rutile TiO_2(110), Chem. Soc. Rev. 37 (2008) 2328−2353.

[2] U. Diebold, The surface science of titanium dioxide, Surf. Sci. Rep. 48 (2003) 53−229.

[3] S. Kielbassa, M. Kinne, R.J. Behm, Thermal stability of Au nanoparticles in O_2 and air on fully oxidized TiO_2(110) substrates at elevated pressures. an AFM/XPS study of Au/TiO_2 model systems, J. Phys. Chem. B 108 (2004) 19184–19190.

[4] M. Eyrich, S. Kielbassa, T. Diemant, J. Biskupek, U. Kaiser, U. Wiedwald, P. Ziemann, J. Bansmann, Planar Au/TiO_2 model catalysts: fabrication, characterization and catalytic activity, Chem. Phys. Chem. 11 (2010) 1430–1437.

[5] S. Dohshi, M. Anpo, S. Okuda, T. Kojima, Effect of γ-ray irradiation on the wettability of TiO_2 single crystals, Topics in Catal. 35 (2005) 327−330.

[6] Y. Yamamoto, K. Nakajima, T. Ohsawa, Y. Matsumoto, H. Koinuma, Preparation of atomically smooth TiO_2 single crystal surfaces and their photochemical property, Jpn. J. Appl. Phys. 44 (2005) L511–L514.

[7] M. Murphy, M.S. Walczak, H. Hussain, M.J. Acres, C.A. Muryn, A.G. Thomas, N. Silikas, R. Lindsay, An ex situ study of the adsorption of calcium phosphate from solution onto TiO_2(110) and Al_2O_3(0001), Surf. Sci. 646 (2016) 146–153.

[8] S. Wendt, R. Schaub, J. Matthiesen, E.K. Vestergaard, E. Wahlström, M.D. Rasmussen, P. Thostrup, L.M. Molina, E. Lægsgaard, I. Stensgaard, B. Hammer, F. Besenbacher, Oxygen vacancies on TiO_2(110) and their interaction with H_2O and O_2: a combined high-resolution STM and DFT study, Surf. Sci. 598 (2005) 226–245.

[9] U. Diebold, J. Lehman, T. Mahmoud, M. Kuhn, G. Leonardelli, W. Hebenstreit, M. Schmid, P. Varga, Intrinsic defects on a TiO_2(110) (1×1) surface and their reaction with oxygen: a scanning tunneling microscopy study, Surf. Sci. 411 (1998) 137–153.

[10] H. Onishi, K. Fukui, Y. Iwasawa, Atomic-scale surface structures of TiO_2(110) determined by scanning tunneling microscopy: a new surface-limited phase of titanium oxide, Bull. Chem. Soc. Jpn. 68 (1995) 2447−2458.

[11] Y. Du, N.A. Deskins, Z. Zhang, Z. Dohnálek, M. Dupuis, I. Lyubinetsky, Imaging consecutive steps of O_2 reaction with hydroxylated TiO_2(110): identification of HO_2 and terminal OH intermediates, J. Phys. Chem. C 113 (2009) 666–671.

[12] A. Sasahara, M. Tomitori, An atomic-scale study of TiO_2(110) surfaces exposed to humid environments. J. Phys. Chem. C 120 (2016) 21427−21435.

[13] M. Li, W. Hebenstreit, U. Diebold, A.M. Tyryshkin, M.K. Bowman, G.G. Dunham, M.A. Henderson, The influence of the bulk reduction state on the surface structure and morphology of rutile TiO_2(110) single crystals, J. Phys. Chem. B 104 (2000) 4944–4950.

[14] A. Sasahara, S. Kitamura, H. Uetsuka, H. Onishi, Oxygen-atom vacancies imaged by a noncontact atomic force microscope operated in an atmospheric pressure of N_2 gas, J. Phys. Chem. B 108 (2004) 15735–15737.

[15] K. Fukui, H. Onishi, Y. Iwasawa, Atom-resolved image of the TiO_2(110) surface by noncontact atomic force microscopy, Phys. Rev. Lett. 79 (1997) 4202–4205.

[16] S. Morita, R. Wiesendanger, E. Meyer (Eds.), Noncontact Atomic Force Microscopy, Springer, Berlin, 2002.

[17] T.T.U. Le, A. Sasahara, M. Tomitori, Water wettability of an ultra-thin layer of silicon oxide epitaxially grown on a rutile titanium dioxide (110) surface, J. Phys. Chem. C 117 (2013) 23621–23625.

[18] A. Sasahara, C.L. Pang, M. Tomitori, Atomic scale analysis of ultra thin SiO_2 films prepared on TiO_2(100) surfaces. J. Phys. Chem. C 114 (2010) 20189–20194.

[19] I. Horcas, R. Fernandez, J.M. Gomez-Rodriguez, J. Colchero, J. Gomez-Herrero, A.M. Baro, WSXM: a software for scanning probe microscopy and a tool for nanotechnology. Rev. Sci. Instrum. 78 (2007) 013705, 1–8.

[20] A. Sasahara, M. Tomitori, XPS and STM study of Nb-doped TiO_2(110)-(1×1) surfaces, J. Phys. Chem. C 117 (2013) 17680−17686.

[21] Petkov, V.; Holzhüter, G.; Tröge, U.; Gerber, Th.; Himmel, B. Atomic-Scale Structure of Amorphous TiO_2 by Electron, X-ray Diffraction and Reverse Monte Carlo Simulations. J. Non-Cryst. Solids 231 (1998) 231, 17–30.

[22] R. Shimizu, K. Iwaya, T. Ohsawa, T. Hasegawa, T. Hashizume, T. Hitosugi, Simplified method to prepare atomically-ordered TiO_2(110)-(1×1) surfaces with steps and terraces, Appl. Surf. Sci. 257 (2011) 4867–4869.

[23] Yanagisawa, K.; Ovenstone, J. Crystallization of Anatase from Amorphous Titania Using the Hydrothermal Technique: Effects of Starting Material and Temperature. J. Phys. Chem. B 103 (1999) 7781–7787.

[24] A. Sasahara, H. Uetsuka, H. Onishi, Noncontact atomic force microscope topography dependent on the electrostatic dipole field of individual molecules, Phys. Rev. B 64 (2001) 121406(R) 1–4.
[25] K. Assaker, C. Carteret, P. Durand, L. Aranda, M. J. Stébé, and J. L. Blin, Hydrothermal Stability of Ordered Surfactant-Templated Titania, J. Phys. Chem. C 117 (2013) 16500−16508.
[26] D. Wang, L. Liu, F. Zhang, K. Tao, E. Pippel, and K. Domen, Spontaneous phase and morphology transformations of anodized titania nanotubes induced by water at room temperature, Nano Lett. 11 (2011) 3649–3655.
[27] B. Prasai, B. Cai, M.K. Underwood, J.P. Lewis, D.A. Drabold, Properties of amorphous and crystalline titanium dioxide from first principles, J. Mater. Sci. 47 (2012) 7515–7521.
[28] H. Zhang, B. Chen, and J.F. Banfield, Atomic structure of nanometer-sized amorphous TiO_2, Phys. Rev. B 78 (2008) 214106, 1–12.

Figure captions

Figure 1. (a) A ball-and-stick model of the TiO_2(110)–(1 × 1) surface. Light blue balls and red balls represent the Ti atoms and O atoms, respectively. The smallest grey balls bonded to the O_b atoms are H atoms. The OH_t group terminating the Ti_{5c} atom is added for reference. The dimensions of the unit cell indicated by the dotted line are 0.30 nm × 0.65 nm. (b,c) FM-AFM images of the TiO_2(110)–(1 × 1) surface prepared in UHV. The dotted rectangle in (c) indicates the unit cell. (b) Scan area (S), 500 nm × 500 nm; frequency shift (Δf), −50 Hz; sample bias (V_s), +1.0 V; peak-to-peak amplitude of the cantilever oscillation ($A_{p\text{-}p}$), 6.4 nm. (c) S, 6 nm × 6 nm; Δf, −205 Hz; V_s, +0.9 V; $A_{p\text{-}p}$, 7.5 nm.

Figure 2. (a,b) FM-AFM images of the air-annealed surface. (a) S, 500 nm × 500 nm; Δf, −10 Hz; V_s, −0.75 V; $A_{p\text{-}p}$, 2.1 nm. (b) S, 50 nm × 50 nm; Δf, −20 Hz; V_s, −0.75 V; $A_{p\text{-}p}$, 2.1 nm. (c) Cross sections along the solid lines in (a) and (b). (d) The LEED pattern of the air-annealed surface. Incident electron energy (E_i), 120 eV. The dotted rectangle indicates a unit cell of the (1 × 1) structure, and arrows indicate the extra spots. (e) A wide-scan XPS spectrum of the air-annealed surface.

Figure 3. (a) A ball-and-stick model of the air-annealed surface. The rutile substrate is covered by amorphous fragments highlighted by the dotted rounded rectangles. Light-blue balls and red balls represent Ti atoms and O atoms, respectively. The OH groups are not depicted for simplification. (b) Structural change of the amorphous fragments (i) and (ii) in (a). TiO_6 octahedral models are presented for the perspective views. (c) A ball-and-stick model of the O_2-annealed surface.

Figure 4. (a,b) FM-AFM images of the air-annealed surface subsequently annealed in O_2. (a) S, 500 nm × 500 nm; Δf, −28 Hz; V_s, +0.8 V; $A_{p\text{-}p}$, 3.0 nm. (b) S, 50 nm × 50 nm; Δf, −38 Hz; V_s, +0.8 V; $A_{p\text{-}p}$, 3.0 nm. A close-up of the terrace is shown in the inset (S, 10 nm × 10 nm; Δf, −28 Hz; V_s, +0.8 V; $A_{p\text{-}p}$, 3.0 nm). The arrows indicates the molecule-sized spots. (c) Cross sections along the solid lines in (a,b). (d) The LEED pattern of the air-annealed surface subsequently annealed in O_2. Here, E_i was 120 eV. The dotted rectangle indicates the unit cell of the (1 × 1) structure. Four of the (2 × 1) spots are indicated by the arrows. (e) Wide-scan XPS spectrum of the air-annealed surface.

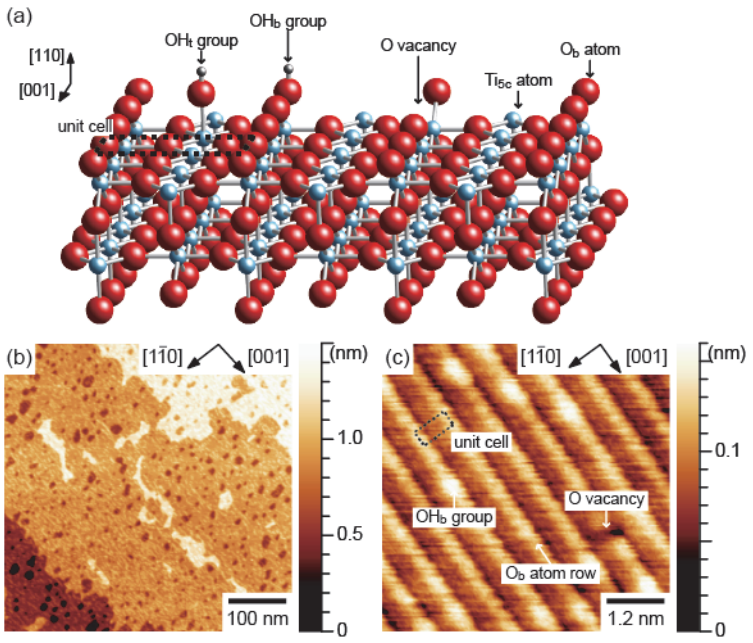

Figure 1. (a) A ball-and-stick model of the TiO_2(110)–(1 × 1) surface. Light blue balls and red balls represent the Ti atoms and O atoms, respectively. The smallest grey balls bonded to the O_b atoms are H atoms. The OH_t group terminating the Ti_{5c} atom is added for reference. The dimensions of the unit cell indicated by the dotted line are 0.30 nm × 0.65 nm. (b,c) FM-AFM images of the TiO_2(110)–(1 × 1) surface prepared in UHV. The dotted rectangle in (c) indicates the unit cell. (b) Scan area (S), 500 nm × 500 nm; frequency shift (Δf), −50 Hz; sample bias (V_s), +1.0 V; peak-to-peak amplitude of the cantilever oscillation ($A_{p\text{-}p}$), 6.4 nm. (c) S, 6 nm × 6 nm; Δf, −205 Hz; V_s, +0.9 V; $A_{p\text{-}p}$, 7.5 nm.

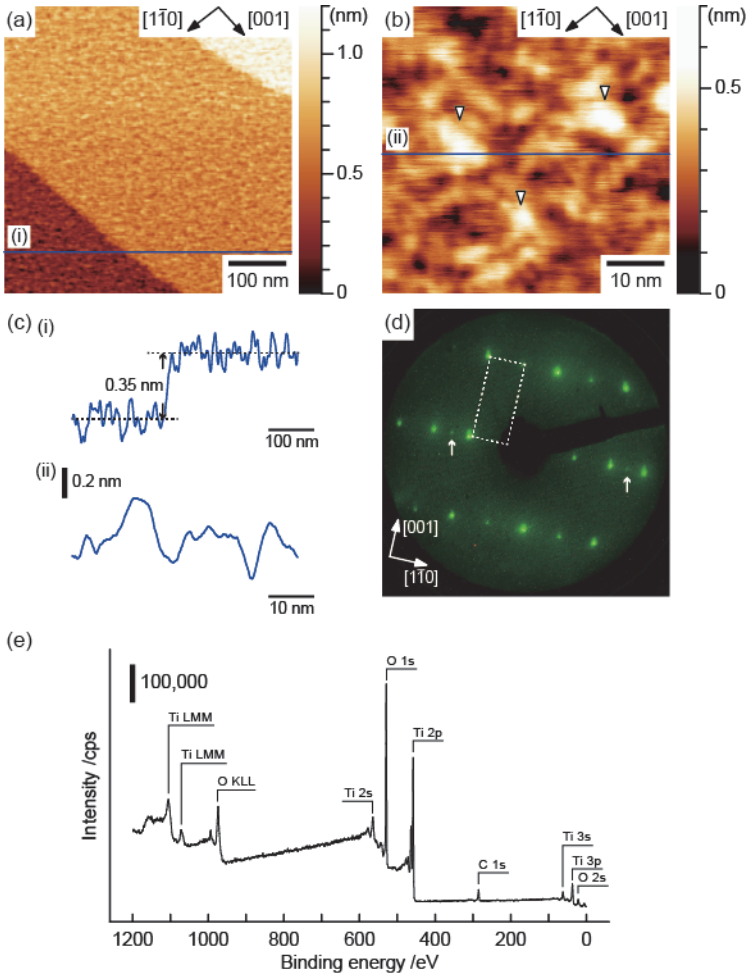

Figure 2. (a,b) FM-AFM images of the air-annealed surface. (a) *S*, 500 nm × 500 nm; Δ*f*, −10 Hz; V_s, −0.75 V; $A_{p\text{-}p}$, 2.1 nm. (b) *S*, 50 nm × 50 nm; Δ*f*, −20 Hz; V_s, −0.75 V; $A_{p\text{-}p}$, 2.1 nm. (c) Cross sections along the solid lines in (a) and (b). (d) The LEED pattern of the air-annealed surface. Incident electron energy (E_i), 120 eV. The dotted rectangle indicates a unit cell of the (1 × 1) structure, and arrows indicate the extra spots. (e) A wide-scan XPS spectrum of the air-annealed surface.

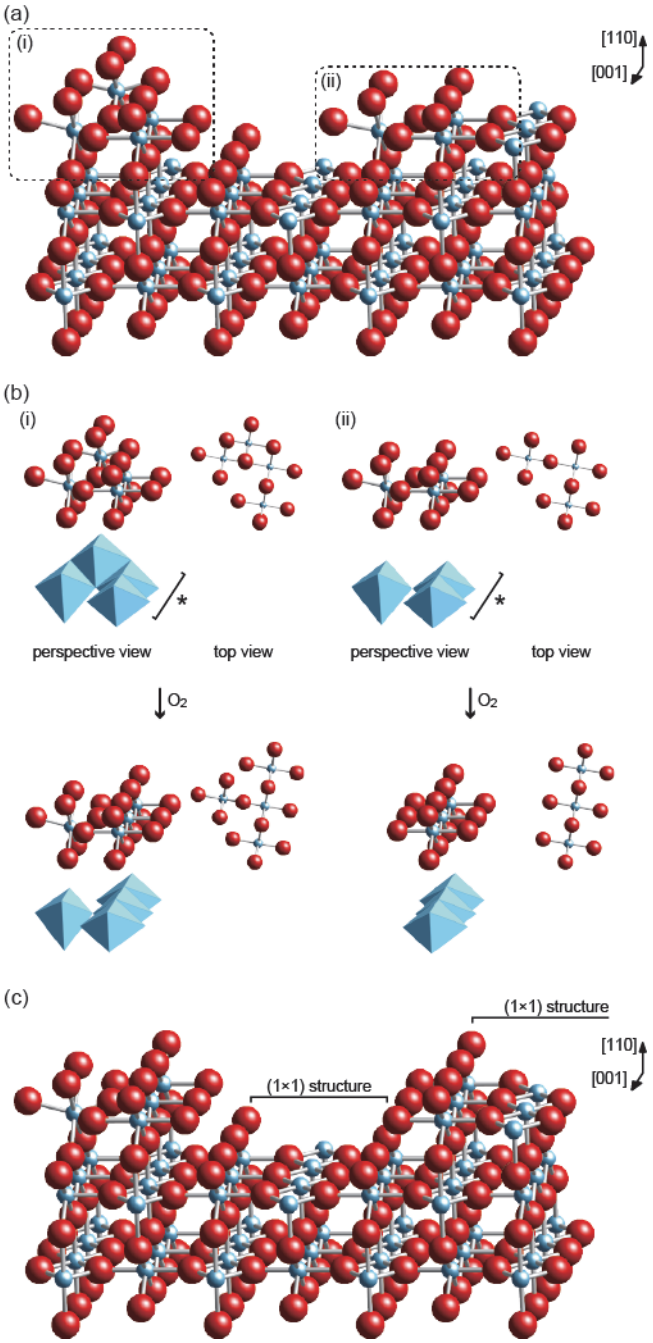

Figure 3. (a) A ball-and-stick model of the air-annealed surface. The rutile substrate is covered by amorphous fragments highlighted by the dotted rounded rectangles. Light-blue balls and red balls represent Ti atoms and O atoms, respectively. The OH groups are not depicted for simplification. (b) Structural change of the amorphous fragments (i) and (ii) in (a). TiO_6 octahedral models are presented for the perspective views. (c) A ball-and-stick model of the O_2-annealed surface.

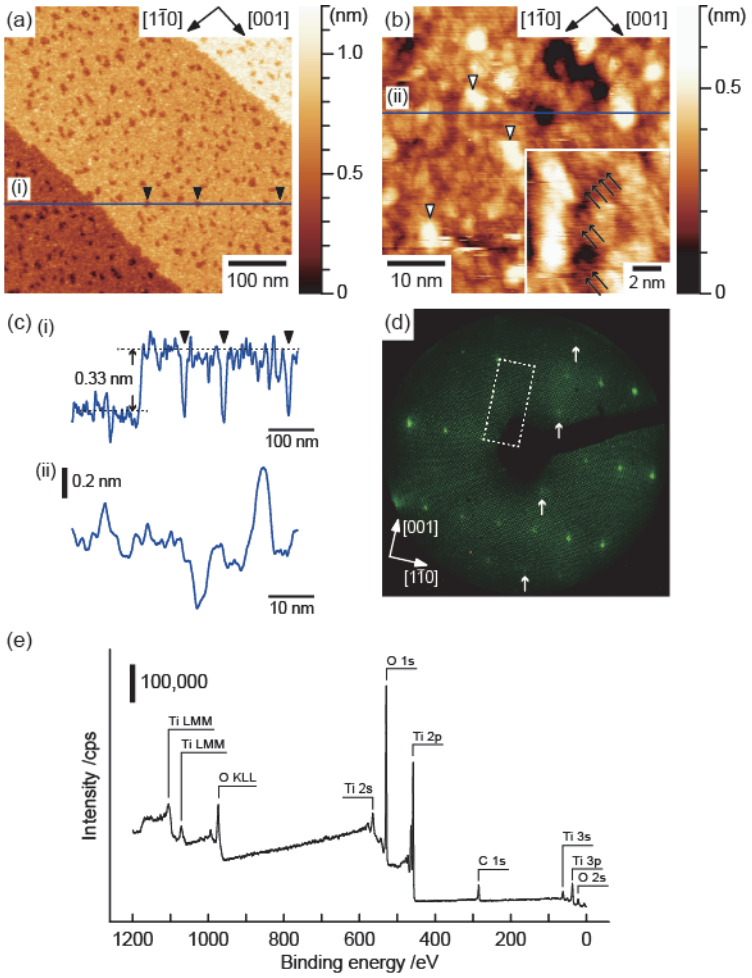

Figure 4. (a,b) FM-AFM images of the air-annealed surface subsequently annealed in O_2. (a) *S*, 500 nm × 500 nm; Δf, −28 Hz; V_s, +0.8 V; $A_{p\text{-}p}$, 3.0 nm. (b) *S*, 50 nm × 50 nm; Δf, −38 Hz; V_s, +0.8 V; $A_{p\text{-}p}$, 3.0 nm. A close-up of the terrace is shown in the inset (*S*, 10 nm × 10 nm; Δf, −28 Hz; V_s, +0.8 V; $A_{p\text{-}p}$, 3.0 nm). The arrows indicates the molecule-sized spots. (c) Cross sections along the solid lines in (a,b). (d) The LEED pattern of the air-annealed surface subsequently annealed in O_2. Here, E_i was 120 eV. The dotted rectangle indicates the unit cell of the (1 × 1) structure. Four of the (2 × 1) spots are indicated by the arrows. (e) Wide-scan XPS spectrum of the air-annealed surface.